Gain-of-function mutations of PPM1D/Wip1 impair the p53-dependent G1 checkpoint

Petra Kleiblova,[1,4] Indra A. Shaltiel,[2,3] Jan Benada,[4,5] Jan Ševčík,[1] Soňa Pecháčková,[4,5] Petr Pohlreich,[1] Emile E. Voest,[3] Pavel Dundr,[6] Jiri Bartek,[5,7,8] Zdenek Kleibl,[1] René H. Medema,[2,3] and Libor Macurek[4,5]

[1]Institute of Biochemistry and Experimental Oncology, First Faculty of Medicine, Charles University in Prague, CZ-12853 Prague, Czech Republic
[2]Division of Cell Biology, The Netherlands Cancer Institute, 1066CX Amsterdam, Netherlands
[3]Department of Medical Oncology, University Medical Center Utrecht, 3584CG Utrecht, Netherlands
[4]Department of Cancer Cell Biology and [5]Department of Genome Integrity, Institute of Molecular Genetics v.v.i., Academy of Sciences of the Czech Republic, CZ-14220 Prague, Czech Republic
[6]Institute of Pathology, First Faculty of Medicine, Charles University in Prague and General University Hospital in Prague, CZ-12000 Prague, Czech Republic
[7]Institute of Molecular and Translational Medicine, Palacky University, CZ-77515 Olomouc, Czech Republic
[8]Danish Cancer Society Research Center, DK-2100 Copenhagen, Denmark

The DNA damage response (DDR) pathway and its core component tumor suppressor p53 block cell cycle progression after genotoxic stress and represent an intrinsic barrier preventing cancer development. The serine/threonine phosphatase PPM1D/Wip1 inactivates p53 and promotes termination of the DDR pathway. Wip1 has been suggested to act as an oncogene in a subset of tumors that retain wild-type p53. In this paper, we have identified novel gain-of-function mutations in exon 6 of *PPM1D* that result in expression of C-terminally truncated Wip1. Remarkably, mutations in *PPM1D* are present not only in the tumors but also in other tissues of breast and colorectal cancer patients, indicating that they arise early in development or affect the germline. We show that mutations in *PPM1D* affect the DDR pathway and propose that they could predispose to cancer.

Introduction

Proliferating cells respond to genotoxic stress by activating a conserved DNA damage response (DDR) pathway that blocks cell cycle progression (checkpoint) and facilitates DNA repair. Activation of ATM (ataxia telangiectasia mutated)/Chk2, ATR (ataxia telangiectasia and Rad3 related)/Chk1, and p38/MK2 kinases converges on the tumor suppressor p53, which plays a central role in regulating cell fate decisions in response to genotoxic stress (Jackson and Bartek, 2009; Medema and Macůrek, 2012). In general, genotoxic stress induces stabilization, oligomerization, and binding of p53 to promoters, causing a widespread modulation of gene expression (Vogelstein et al., 2000). Although high doses of DNA damage (such as therapeutic irradiation or radiomimetic drugs) lead to p53-induced programmed cell death or permanent withdrawal from the cell cycle (senescence), more moderate DNA damage (originating from erroneous DNA metabolism or from environmental factors) triggers expression of DNA repair genes and a cyclin-dependent kinase inhibitor p21(WAF1/CIP1) that controls the G1 checkpoint (el-Deiry et al., 1993). After completion of DNA repair, cells recover from the temporal checkpoint arrest and return to the proliferation program. Wip1 (also known as PPM1D) is a monomeric serine/threonine phosphatase of the PP2C family, and its expression is increased after DNA damage (Fiscella et al., 1997). Wip1 has been implicated in dephosphorylation of multiple DDR components, including ATM, Chk1/2, γ-H2AX, and p53, all contributing to timely inactivation of DDR after DNA repair (Le Guezennec and Bulavin, 2010). In addition, Wip1-dependent inactivation of p53 is thought to play a major role in control of checkpoint recovery (Lindqvist et al., 2009).

Recent work has identified oncogene-induced replication stress and DNA breakage that trigger the DDR as an intrinsic barrier against progression of early preinvasive stages of solid tumors to malignant lesions (Bartkova et al., 2005, 2006; Gorgoulis et al., 2005; Di Micco et al., 2006; Halazonetis et al., 2008). According to this model, cells that accumulate mutations circumventing the checkpoint barrier have a selective advantage

P. Kleiblova and I.A. Shaltiel contributed equally to this paper.

Correspondence to Libor Macurek: libor.macurek@img.cas.cz; or René H. Medema: r.medema@nki.nl

Abbreviations used in this paper: DDR, DNA damage response; FL, full length; FUCCI, fluorescent, ubiquitination-based cell cycle indicator; IR, ionizing radiation; IRIF, IR-induced foci; MS, mass spectrometry; STLC, S-trityl-L-cysteine.

The Rockefeller University Press $30.00
J. Cell Biol. Vol. 201 No. 4 511–521
www.jcb.org/cgi/doi/10.1083/jcb.201210031

and can thus promote further development of cancer. The most common example of such DDR defect is an inactivating somatic mutation in the *TP53* gene that disables proper response to genotoxic stress, leads to genomic instability, and is found in about half of human tumors (Hollstein et al., 1991). On the other hand, tumors that retain wild-type p53 are likely to accumulate other genetic defects that would allow them to overcome the DDR barrier, providing a growth advantage in the presence of replicative stress. Importantly, amplification of the 17q23 locus carrying the *PPM1D* gene has been reported in various p53 wild-type tumors, pointing toward a role of Wip1 in cancer development, and Wip1 overexpression is associated with poor prognosis (Bulavin et al., 2002, 2004; Li et al., 2002; Saito-Ohara et al., 2003; Rauta et al., 2006; Castellino et al., 2008; Liang et al., 2012). The oncogenic behavior of Wip1 is further supported by mouse genetics showing that loss of Wip1 protects from cancer development (Bulavin et al., 2004; Nannenga et al., 2006). However, point mutations that affect Wip1 function have not been reported. Here, we have identified novel truncating mutations of Wip1 that show a gain-of-function effect and impair p53-dependent responses to genotoxic stress. Strikingly, mutations in the *PPM1D* gene were found also in breast and colorectal cancer patients, suggesting that such truncating mutations of Wip1 may predispose to a wider range of cancer types.

Results and discussion

Because amplification of the *PPM1D* gene occurs mainly in tumors that retain the wild-type p53, we have screened a panel of p53-proficient tumor cell lines to determine the expression level of Wip1 in tumors derived from various tissues (Bulavin et al., 2002; Rauta et al., 2006). Predictably, we could confirm high expression of Wip1 in MCF7 cells that are known to carry an extensive amplification of the *PPM1D* locus (Fig. 1 A; Pärssinen et al., 2008). All other tested cell lines expressed substantially lower amounts of full-length (FL) Wip1. Surprisingly, we noticed an abundant, faster migrating band, recognized by two distinct Wip1 antibodies in HCT116 and U2OS cells derived from colorectal adenocarcinoma and osteosarcoma, respectively (Fig. 1, A and B). Notably, antibodies recognizing an epitope corresponding to the amino acid residues 380–410 of Wip1 stained both bands, whereas an antibody directed against an epitope corresponding to the amino acid residues 500–550 of Wip1 recognized only the slower migrating band (Figs. 1 A and S1 A). In addition, both bands were depleted by three independent Wip1 siRNAs, indicating that the two protein bands correspond to various forms of Wip1 (Fig. S1 B). Consistent with this, sequencing of genomic DNA revealed heterozygous mutations (c.1349delT and c.1372C>T) within exon 6 of the *PPM1D* gene that caused truncation of the Wip1 protein (p.L450X in HCT116 and p.R458X in U2OS cells; Fig. 1 C). Expression of both the FL and truncated versions of Wip1 in U2OS and HCT116 cells was further confirmed by immunopurification of Wip1 and subsequent mass spectrometry (MS) analysis (Fig. S1, C and D). Importantly, epitope-tagged versions of truncated Wip1 proteins expressed from plasmid DNA showed electrophoretic mobility that closely resembled that of the aberrant endogenous Wip1 proteins (Fig. S1 E).

To understand whether truncation of Wip1 affects its function in the DDR, we asked whether the respective truncation mutants were capable of suppressing formation of ionizing radiation (IR)–induced foci (IRIF) as has been described for FL Wip1 (Macůrek et al., 2010). Both, Wip1-L450X and Wip1-R458X localized properly in the nucleus and were bound to the chromatin, suggesting that overall subcellular distribution of Wip1 is not affected by the exon 6 truncations (Fig. 2 A). As expected, overexpression of FL-Wip1 resulted in a reduction in IRIF formation, as determined by the number of 53BP1 foci induced after irradiation (Fig. 2 B). Similarly, overexpression of Wip1-L450X and Wip1-R458X (but not phosphatase-dead Wip1-D314A) also caused a dramatic reduction in IRIF formation, suggesting that the mutants retain normal phosphatase activity that opposes IRIF assembly (Fig. 2 B). In addition, expression of FL-Wip1, Wip1-L450X, and Wip1-R458X significantly decreased levels of radiation-induced phosphorylation of histone H2AX (γ-H2AX) and pSer15-p53 (both established markers of DDR and substrates of Wip1; Lu et al., 2005; Macůrek et al., 2010), suggesting that all tested Wip1 proteins are capable of silencing the DDR (Fig. 2 C). Wip1 is a monomeric phosphatase, and because all identified truncating mutations reside in the C-terminal region of Wip1 leaving the N-terminal catalytic domain intact, we hypothesized that the truncation mutants retain phosphatase activity. Indeed, immunopurified FL-Wip1, Wip1-L450X, and Wip1-R458X showed comparable phosphatase activity in vitro, and therefore, it is unlikely that mutation of *PPM1D* leads to production of a hyperactive Wip1 (Fig. 2 D).

Because mutations in oncogenes are expected to cause a gain-of-function effect, we wondered whether the C-terminal region coded by exon 6 reduces the stability of Wip1. Consistent with this notion, we found that both U2OS and HCT116 cells expressed ∼10–20-fold more of the truncated Wip1 compared with the FL-Wip1 (Fig. 2 E). In contrast, no substantial differences between wild-type and mutated Wip1 expression were found at the mRNA level, indicating that these are not differentially regulated at the transcriptional level and that the high levels of the mutant Wip1 proteins reflect enhanced protein stability (Fig. S1 F). Indeed, the FL-Wip1 disappeared rapidly after treatment of cells with cycloheximide (half-life of 1–2 h), whereas both truncated mutants exhibited enhanced stability (half-life of >6 h; Fig. 3, A and B). In addition, treatment with the proteasomal inhibitor MG-132 reversed the effect of the cycloheximide on destabilization of the FL-Wip1 (Fig. 3 C). This suggests that the C-terminal domain of Wip1 somehow renders the FL protein unstable and that its turnover is regulated by the proteasome. To further corroborate this notion, we fused the C-terminal noncatalytic part of Wip1 (aa 380–605) to GFP and analyzed its effect on protein stability. Similar to what we observed for FL-Wip1, we found that the GFP fusion containing the C-terminal tail of Wip1 was less stable than GFP itself (Fig. 3 D). From this, we conclude that nonsense mutations in exon 6 of the *PPM1D* gene lead to increased protein levels of enzymatically active truncated Wip1 and thus result in increased total Wip1 activity in cells.

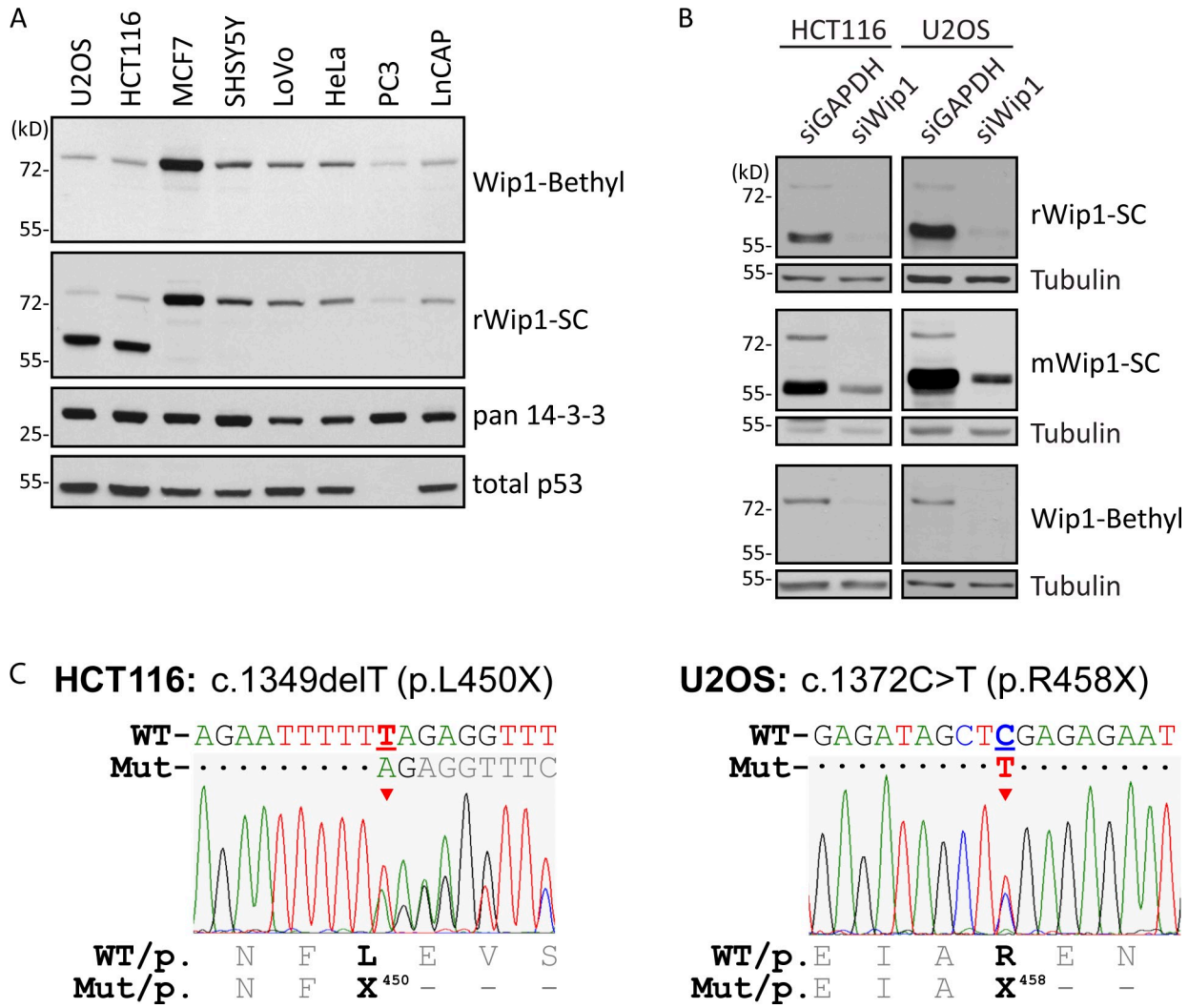

Figure 1. **The *PPM1D* gene is mutated in selected cancer cell lines.** (A) Whole-cell lysates from indicated cell lines were probed with anti-Wip1 (Bethyl Laboratories, Inc.), anti-Wip1 (Santa Cruz Biotechnology, Inc. [SC]), and anti–14-3-3 (loading control) antibodies. Note the additional Wip1-reactive band around 60 kD in U2OS and HCT116 cells. PC3 cells are p53 negative and served as a control. (B) Wip1 was depleted in U2OS and HCT116 cells by siRNA, and lysates were probed with the indicated antibodies. (C) Sequencing chromatograms of *PPM1D* from genomic DNA isolated from U2OS and HCT116 cells. Numbering is based on NCBI GenBank reference sequence NT_010783.15. Mutations are indicated by arrowheads and underlined. WT, wild-type *PPM1D*; Mut, mutated *PPM1D*; c., nucleotide sequence; p., Wip1 peptide sequence.

Despite the fact that U2OS and HCT116 contain wild-type p53, they fail to arrest in G1 in response to IR and preferentially arrest in the G2 checkpoint that remains intact (Fig. S2, A and B). This is reminiscent of the behavior of cells lacking p53 or expressing mutant p53 and suggests that the p53 pathway is somehow compromised in U2OS and HCT116 cells. To test whether this may be caused by enhanced Wip1 levels and/or activity, we depleted Wip1 by RNAi and measured the ability of cells exposed to IR to arrest in G1. Indeed, we observed that U2OS cells did arrest in G1 after depletion of Wip1 and exposure to IR (Figs. 4 A and S2 C). Moreover, this arrest was fully dependent on p53 because codepletion of Wip1 and p53 or depletion of Wip1 in p53-negative cell lines SW480, DLD1, and HT29 did not restore any G1 checkpoint function (Fig. 4 A and not depicted). In addition, depletion of the truncated Wip1 (but not of the FL-Wip1) by isoform-specific RNAi was sufficient to rescue the G1 arrest in irradiated U2OS cells, thus further supporting the conclusion that expression of the truncated variant of Wip1 abrogates the G1 checkpoint (Fig. 4 B). As an alternative approach, we followed the progression from G1 to S phase by time-lapse analysis of living HCT116 cells expressing fluorescent markers to monitor cell cycle progression (Fig. 4 C). HCT116 cells treated with control siRNA were delayed in G1 after irradiation (Fig. 4 C), consistent with previous observations that degradation of Cdc25A and Cyclin D1 can delay S-phase entry in a p53-independent manner (Agami and Bernards, 2000; Mailand et al., 2000). However, the majority of control cells eventually entered S phase (Fig. 4 C). In contrast, HCT116 cells depleted of Wip1 mounted a lasting G1 checkpoint arrest (Fig. 4 C). In accordance with restoration of p53 function upon depletion of Wip1, we observed increased levels of p21 after exposure to IR in U2OS and HCT116 cells treated with Wip1 RNAi (Fig. 4, D and E).

We conclude that cells with mutations that enhance Wip1 protein stability are unable to engage p53 function, fail to arrest

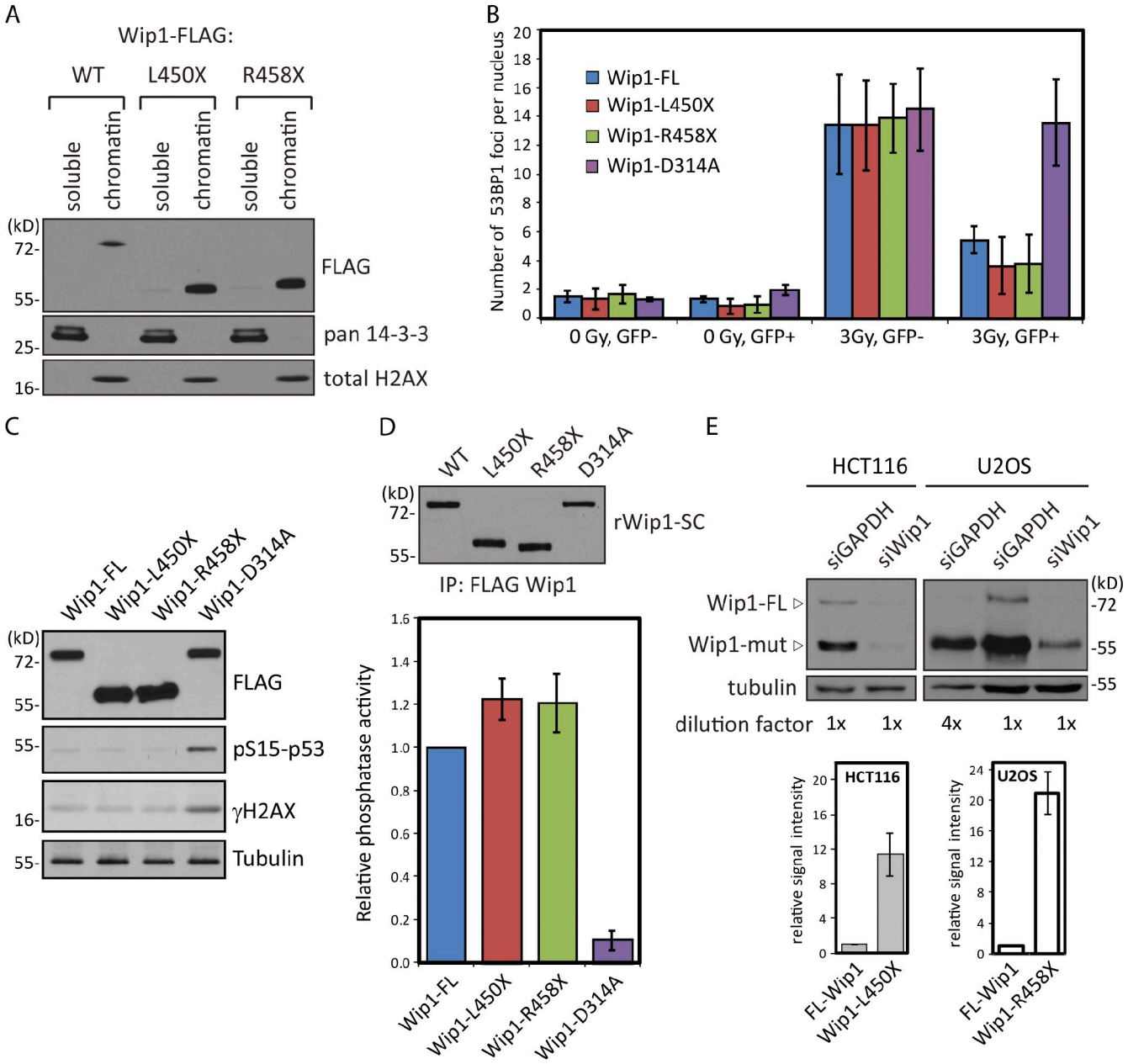

Figure 2. **Truncated Wip1 mutants are enzymatically active.** (A) Soluble and chromatin fractions from cells expressing FL or truncated FLAG-Wip1 were probed with the indicated antibodies. (B) Cells expressing EGFP-Wip1-FL (FL), EGFP-Wip1-D314A (phosphatase dead), or truncated EGFP-Wip1 were fixed 3 h after irradiation (3 Gy). 53BP1 nuclear foci were counted by automated image analysis (1,000 cells per condition). Average number of 53BP1 foci per nucleus in transfected (GFP+) and neighboring control cells (GFP−) is shown. (C) Expression of Wip1-FL, Wip1-D314A, or truncated FLAG-Wip1 was induced by tetracycline 12 h before irradiation (3 Gy). Whole-cell lysates were probed with the indicated antibodies. (D) Phosphatase activity of immunopurified FLAG-Wip1-FL, -L450X, -R458X, or -D314A (phosphatase dead) was measured in vitro using a synthetic phosphopeptide corresponding to pSer15-p53 (bottom), and the precipitated material was probed with anti-Wip1 antibody as a control of equal loading (top). $n = 4$. (E) Quantification of the signal intensity corresponding to the endogenous levels of FL and truncated Wip1 in HCT116 and U2OS cells. siRNA of Wip1 was used as a control of the signal specificity. Error bars indicate standard deviations. mut, mutated; WT, wild type.

in G1 after DNA damage, and progress to S phase. Thus, the genome integrity of cells expressing truncated Wip1 versions may be compromised by replication of the genome that contains unrepaired DNA lesions, including the highly pro-oncogenic DNA double-strand breaks. Increased expression of truncated Wip1 impairs the cellular responses to genotoxic stress also via a reduction in H2AX phosphorylation, which is an established substrate of Wip1. In addition, it is likely that high levels of truncated Wip1 may also directly cause accumulation of mutations through the described negative role of Wip1 in regulation of nucleotide excision repair (Nguyen et al., 2010). All these mechanisms may contribute to the elimination of the intrinsic DDR-mediated barrier against tumor development in cells carrying gain-of-function mutations of Wip1.

Finally, we wished to address the clinical relevance of the identified Wip1 mutations. We therefore performed mutational

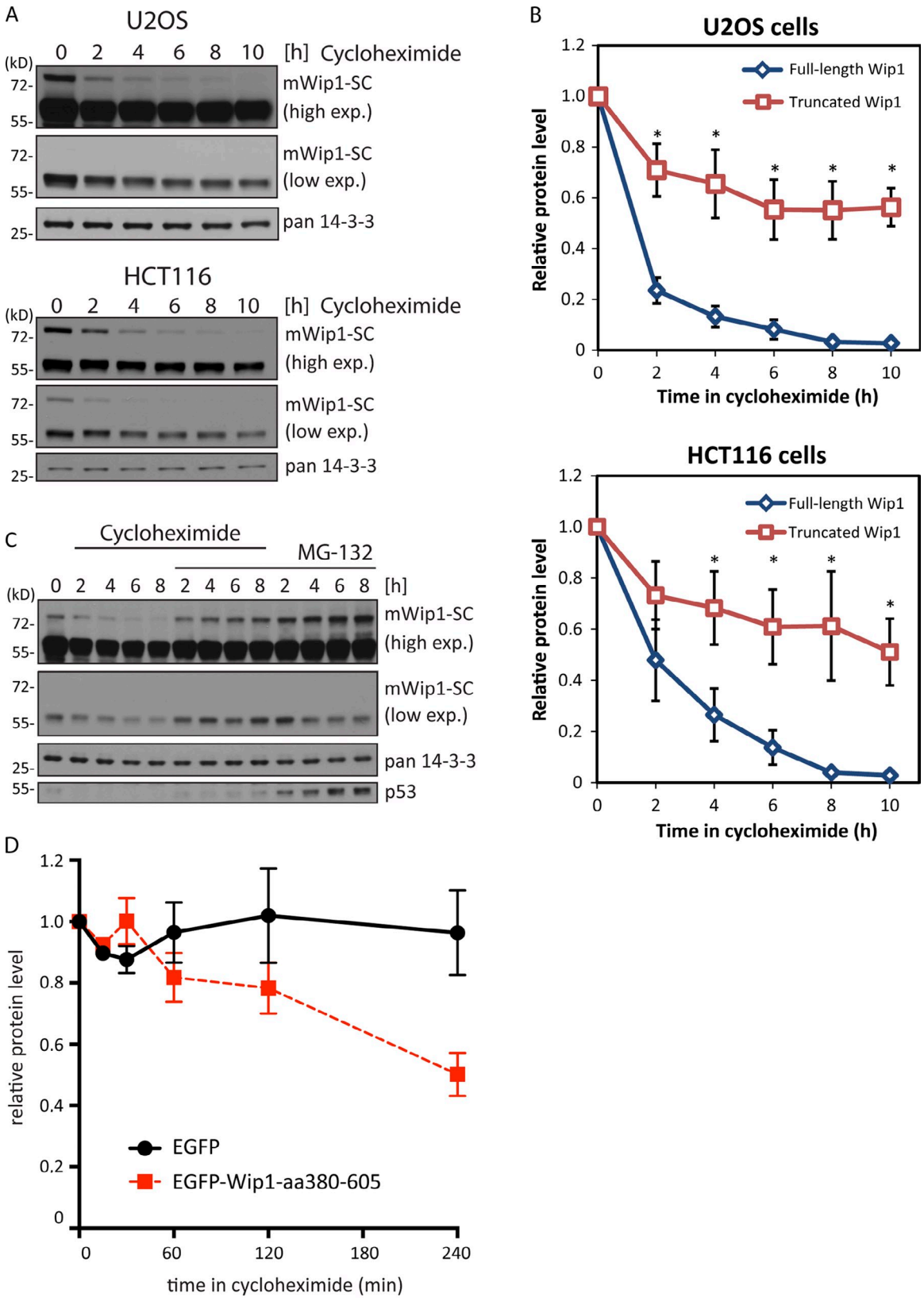

Figure 3. **Truncated Wip1 mutants show increased protein stability.** (A) HCT116 and U2OS cells were treated for the indicated times with cycloheximide. Normalized cell lysates were probed using the monoclonal anti-Wip1 antibody (Santa Cruz Biotechnology, Inc. [SC]). (B) Signal intensity corresponding to the FL-Wip1 and truncated Wip1 from A was quantified using ImageJ software. The relative change in signal intensity is shown. Statistical significance was determined by unpaired two-tailed *t* test ($n = 3$; *, $P < 0.05$). (C) U2OS cells were treated with cycloheximide, proteasomal inhibitor MG132 or a combination of both for the indicated times and analyzed as in A. (D) U2OS cells were transfected with plasmid DNA coding for EGFP or EGFP fused to the C-terminal region of Wip1 (aa 380–605). Cells were treated for the indicated times with cycloheximide. Normalized cell lysates were probed with an anti-GFP antibody, and the signal intensity was quantified using ImageJ software. $n = 3$. Error bars indicate standard deviations. exp., exposure.

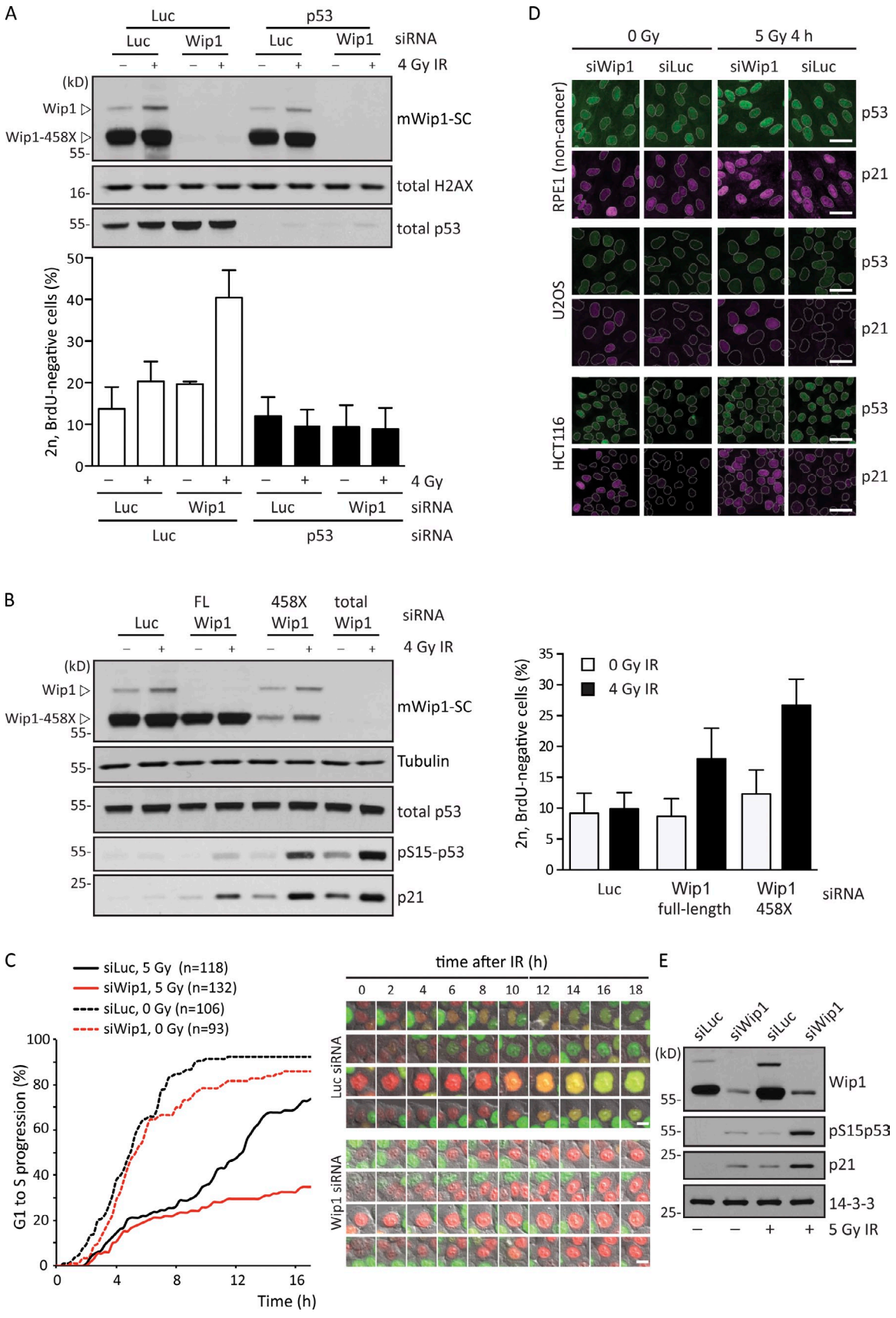

Figure 4. **Mutated Wip1 impairs the p53-dependent G1 checkpoint.** (A) U2OS cells were transfected by siRNA targeting luciferase, Wip1 and/or p53 and grown for 48 h. Cells were treated with BrdU and STLC, irradiated or not irradiated with 4 Gy, and grown for a further 16 h. Cells were analyzed by immunoblotting (top) or by flow cytometry (bottom) to determine the fraction of G1 cells (2n; BrdU negative). (B) U2OS cells were transfected by

analysis of the *PPM1D* gene in a panel of unselected colorectal cancer patients (n = 304) and a panel of high-risk patients with *BRCA1/2*-negative breast and ovarian cancer (n = 728) and identified four deleterious mutations in exon 6 (c.1372C>T and c.1602insT in patients with colorectal cancer and c.1601del15 and c.1451T>G in patients with breast cancer) compared with no such mutations present in noncancer control samples (n = 450; Fig. 5 A and Table S1). All identified Wip1-truncating mutations (p.R458X, p.L484X, p.K535X, and p.F534X) and showed a striking similarity to mutations identified in the tumor cell lines. Functional analysis of all Wip1 mutants present in cancer patients confirmed that these truncations retain the enzymatic activity as well as the ability to bind to chromatin (Fig. 5, B and C; and not depicted). In addition, we analyzed protein levels of Wip1 in leukocytes in one of the mutant carriers and found that the truncated Wip1 is expressed at a much higher level than the FL-Wip1, thus phenocopying the situation in tumor cell lines (Fig. 5 D). Finally, we analyzed a noncancer mammary tissue and tumor tissue from one mutation carrier and identified a heterozygous mutation in the tumor tissue (Fig. 5 E).

Remarkably, all truncating mutations identified in the *PPM1D* gene in patients and cancer cell lines were heterozygous gain-of-function mutations, which is consistent with the role of Wip1 as an oncogene. Of note, alterations in cancer patients were identified in peripheral blood samples, excluding the possibility that these mutations arise in the developing tumor simply as a consequence of genetic instability. The targeting to a discrete hot-spot region in the exon 6 of the *PPM1D* oncogene—their gain-of-function character proven by in vitro experiments—the variable onset of cancer in affected individuals, and the versatile spectrum of cancer types appearing in mutation carriers and cancer cell lines all indicate that mutations in *PPM1D* may represent an unusual and novel genetic risk factor of general cancer predisposition not associated with a single specific cancer type.

Although the majority of hereditary cancers is caused by mutations in tumor suppressor genes, germline mutations in oncogenes are not unprecedented (Knudson, 2002). For example, germline mutations of oncogenic tyrosine kinases *RET*, *MET*, and *KIT* are linked with medullary thyroid carcinoma, hereditary papillary renal carcinoma, and hereditary gastrointestinal stromal tumor syndrome, respectively (Mulligan et al., 1993; Schmidt et al., 1997; Nishida et al., 1998). Whereas tumor development is substantially boosted by inactivation of the second allele of the tumor suppressor genes, monoallelic gain-of-function mutations are usually sufficient to activate oncogenes (Vogelstein and Kinzler, 2004). In agreement with this, identified mutations of *PPM1D* in the tumor cell lines were heterozygous, and both wild-type and truncated *PPM1D* alleles were expressed. We propose that the high expression level of truncated Wip1 impairs the p53-dependent genome surveillance system in mutation carriers, making their genomic DNA hypersensitive to various genotoxic insults. By this mechanism, mutations in other tumor-promoting genes may accumulate throughout the entire life span of the *PPM1D* mutation carriers and promote cancer development. The clinical significance of truncating *PPM1D* mutations in predisposition to breast and ovarian cancer was recently documented by an extensive case control study (Ruark et al., 2013). Further studies are needed to address the possibility that mutations in *PPM1D* may represent a hereditary cancer predisposition and that truncated Wip1 might be a suitable candidate for pharmacological intervention in cancer patients carrying *PPM1D* mutations.

Materials and methods

Antibodies

Antibodies used were rabbit anti-Wip1 (H300), mouse anti-Wip1 (F-10), anti-p53 (DO1), anti-p21 (C19), and anti-53BP1 (Santa Cruz Biotechnology, Inc.); anti-PPM1D (A300-664A; Bethyl Laboratories, Inc.); anti-pSer15p53, anti-p53, and anti-pSer139-H2AX (Cell Signaling Technology); anti–α-tubulin and anti-FLAG (Sigma-Aldrich); anti-BrdU (clone BU1/75; Abcam); and Alexa Fluor–conjugated secondary antibodies (Life Technologies).

Plasmids

DNA fragments coding for FLAG-tagged human FL or truncated (R458X, L450X, and F534X) Wip1 were generated by PCR and subcloned into BamHI–XbaI sites of the pcDNA4/TO plasmid. Alternatively, coding sequence for EGFP was inserted in HindIII site of pcDNA4/TO and FL, or truncated Wip1 was cloned in frame into BamHI–XbaI sites.

Cell culture

Human U2OS, HCT116, LoVo, MCF7, HeLa, SH-SY5Y, and PC3 or nontumor diploid retinal pigment epithelium cells were grown in DMEM (Gibco) supplemented with 10% FCS, 2 mM L-glutamine, 100 U/ml penicillin, and 100 µg/ml streptomycin. Tetracycline repressor–expressing U2OS-TR cells were grown in media containing tetracycline system–approved FCS, and protein expression was induced by tetracycline. A stable cell line expressing the fluorescent, ubiquitination-based cell cycle indicator (FUCCI) was generated by transduction of HCT116 cells with pCSII-EF-MCS-mKO2-hCdt1(30–120) and pCSII-EF-MCS-mAG-hGeminin(1–110) plasmids (Sakaue-Sawano et al., 2008) followed by FACS sorting of double-positive cells from which a single clone was expanded. Transfections of plasmid DNA were performed using a standard calcium phosphate technique. ON-TARGET*plus* siRNAs targeting Wip1 (5′-GGCCAAGGGUGAAUUCUAA-3′, 5′-CGAAAUGGCUUAAGUCGAA-3′, and 5′-AGUAACGUCCUCCAUGUAC-3′) and control siRNAs (Thermo Fisher Scientific) were transfected (5–10 nM) using RNAiMAX (Invitrogen). Alternatively, isoform-specific siRNAs targeting the FL-Wip1 (5′-AUAGCUCGAGAGAAUGUCC-3′) or the 458X-Wip1 (5′-AUAGCUUGAGAGAAUGUCC-3′) were used.

Immunofluorescence and microscopic analysis

Cells cultured on glass coverslips were left untreated or exposed to IR (dose 3–5 Gy as indicated) and fixed at the indicated times by 4% formaldehyde for 10 min at RT, permeabilized by ice-cold methanol, blocked with 3% BSA in PBS supplemented with 0.1% Tween 20, and incubated with the primary antibodies 60 min at RT. After washing, coverslips were

siRNA targeting various isoforms of Wip1, irradiated, and probed with the indicated antibodies (left) or analyzed by cytometry (right). The fraction of BrdU-negative 2n cells corresponds to cells arrested in G1. (C, left) FUCCI-expressing HCT116 cells were transfected with Wip1 or luciferase siRNA (siLuc), irradiated (4 Gy), and followed by live-cell imaging. Cumulative progression into S phase was determined based on the loss of FUCCI-G1 marker (red) and appearance of the FUCCI-S/G2 marker (green) Numbers of analyzed cells are indicated in parentheses. (right) Representative images of four individual cells transfected with Wip1 or Luciferase siRNA are shown. Bars, 10 µm. (D) Retinal pigment epithelium (RPE1), U2OS, and HCT116 cells were transfected with Wip1 or luciferase siRNA and grown for 48 h before irradiation (5 Gy). Cells were fixed 4 h after IR and probed for total p53 and p21. Bars, 50 µm. (E) U2OS cells were treated as in D, collected 6 h after IR, and probed with the indicated antibodies. SC, Santa Cruz Biotechnology, Inc.

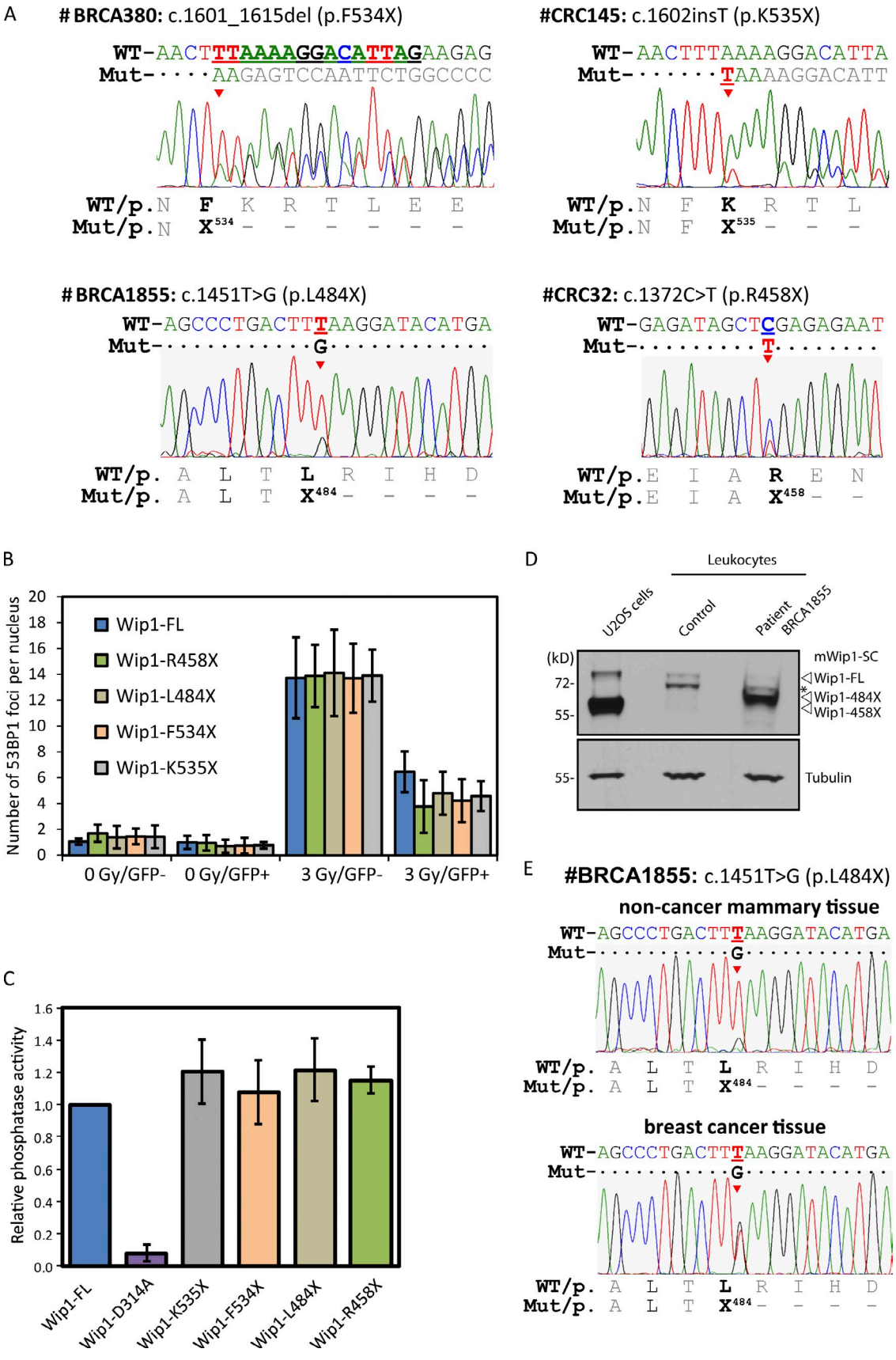

Figure 5. **Truncation mutations of Wip1 are present in cancer patients.** (A) Chromatograms of four truncating mutations identified by screening of the *PPM1D* gene in cancer patients. Mutations are indicated by arrowheads and underlined. WT, wild-type *PPM1D*; Mut, mutated *PPM1D*; c., nucleotide sequence; p., Wip1 peptide sequence. (B) Cells expressing EGFP–Wip1-FL, -R458X, -L484X, -F534X, or -K535X mutants were irradiated, and the number

incubated with Alexa Fluor–conjugated secondary antibodies and mounted using Vectashield reagent (Vector Laboratories) supplemented with 1 µg/ml DAPI. Imaging was performed on DeltaVision Imaging System using NA 1.4 objectives (Applied Precision). Automated image acquisition was performed using a high-content screening station (Scan^R; Olympus; using charge-coupled device camera [IX81 and ORCA-285; Olympus]) equipped with a 40×/1.3 NA objective (RMS40X-PFO; Olympus). Nuclei were identified based on the DAPI signal, and the average number of 53BP1 foci was determined using a spot detection module. At least 1,000 nuclei were counted per condition in three independent experiments. Cells transiently transfected with FL- or mutant EGFP-Wip1 were gated according to the EGFP signal, and neighboring EGFP-negative cells were used as controls. Alternatively, HCT116-FUCCI cells were grown at 37°C in Lab-Tek II chamber slides in L15 media (Gibco) containing all supplements. Cells were irradiated or not irradiated, and videos were acquired using DeltaVision system equipped with a 10×/0.40 NA U-Plan S-Apochromat objective (Olympus), a camera (CoolSNAP HQ2; Photometrics), Quad-mCherry polychroic filter, and mCherry/GFP emission filter sets. Nuclei negative for Geminin-mAG1 (corresponding to G1) directly after irradiation were followed until the appearance of Geminin-mAG1 signal (corresponding to S) detectable over background in two consecutive frames (15 min).

Immunoprecipitation and in vitro phosphatase assay

U2OS cells were extracted by EBC buffer (50 mM Tris, pH 7.5, 150 mM NaCl, 0.5% NP-40, and 1 mM EGTA) followed by sonication (3 × 10 s) and spinning down (20,000 *g* for 10 min). Polyclonal anti-Wip1 (H300; 2 µg/reaction) antibody was incubated with 30 µl protein A/G resin (UltraLink; Thermo Fisher Scientific) and with cell extracts for 4 h at 4°C. As specificity controls, cell extract was incubated with empty beads, and alternatively immobilized antibody was not incubated with cell extract. After extensive washing, beads were mixed with SDS sample buffer and boiled. Immunoprecipitates were probed with polyclonal anti-Wip1 (Bethyl Laboratories, Inc.) and monoclonal anti-Wip1 (Santa Cruz Biotechnology, Inc.). Alternatively, the gel was stained by Coomassie brilliant blue, and immunoprecipitated bands were subjected to MS analysis. Normalized cell extracts from cells expressing FL or truncated FLAG-Wip1 were incubated with M2 agarose (Sigma-Aldrich). In vitro phosphatase assay was performed in a phosphatase buffer (40 mM Hepes, pH 7.4, 100 mM NaCl, 50 mM KCl, 1 mM EGTA, and 50 mM $MgCl_2$) supplemented with 100 µM VEPPLpSQETFS synthetic phosphopeptide (GenScript). Release of phosphate was measured after incubation at 30°C for 20 min using BIOMOL Green reagent (Enzo Life Sciences) and was described previously (Macůrek et al., 2010). Finally, beads containing all immunoprecipitated material were separated by SDS-PAGE and probed for Wip1.

Subcellular fractionation

Soluble and chromatin fractions were prepared as previously described (Macůrek et al., 2010). In brief, soluble cytosolic proteins were extracted from U2OS cells by incubating cells in buffer A (10 mM Hepes, pH 7.9, 10 mM KCl, 1.5 mM $MgCl_2$, 0.34 M sucrose, 10% glycerol, 1 mM DTT, 0.1% Triton X-100, and protease inhibitor cocktail) at 4°C for 10 min and spinning down at 1,500 *g* for 2 min. Soluble nuclear fraction was obtained by extraction of cell nuclei with an equal amount of buffer B (10 mM Hepes, pH 7.9, 3 mM EDTA, 0.2 mM EGTA, and 1 mM DTT) and spinning down at 2,000 *g* for 2 min. Both soluble fractions were mixed (1:1). Insoluble chromatin was washed with buffer B and finally resuspended in SDS sample buffer.

Flow cytometry analysis

Asynchronous cells were transfected with indicated siRNAs (20 nM) and cultured for 48 h before γ-irradiation. To allow determination of cell cycle progression, cells were grown further for 16 h in the presence of 10 µM BrdU and 10 µM S-trityl-L-cysteine (STLC). Cells were collected by trypsinization and either lysed in SDS sample buffer for Western Blot or fixed in ice-cold ethanol for flow cytometry. After incubation in 2M hydrochloric acid and 0.1% Triton X-100, cells were stained with anti-BrdU (replication marker) and anti-mpm2 (mitotic marker) followed by incubation with Alexa Fluor–coupled secondary antibodies. DNA was stained with propidium iodide. Flow cytometry was performed on a cytometer (FACSCalibur; BD), and single cells were analyzed with CellQuest software (BD). As STLC inhibits mitotic kinesin Eg5, cells that progress into mitosis remain arrested in mitosis. This allows identification of cells that were in G1 at the time of IR and remained arrested in the G1 checkpoint (2n DNA content, $BrdU^-mpm2^-$), cells that were in G1/S and progressed to G2 (4n DNA content, $BrdU^+mpm2^-$), cells that were in G1/S and progressed to mitosis (4n DNA content, $BrdU^+mpm2^+$), cells that were in G2 and remained arrested in the G2 checkpoint (4n DNA content, $BrdU^-mpm2^-$), and cells that were in G2 and progressed to mitosis or were in mitosis at the start of the experiment (4n DNA content, $BrdU^-mpm2^+$). The 4n BrdU-negative populations were used to exclude differences in cell cycle distribution at the moment of irradiation. 2n $BrdU^-$ populations were used for quantification of cells remaining in G1. Alternatively, cells were pulsed with 10 µM BrdU (15 min) before irradiation, and BrdU-positive cells were assayed for progression through the G2 phase by FACS analysis of the DNA content (Chen et al., 2001).

Protein stability assay

Cells treated for the indicated times with 50 µg/ml cycloheximide were lysed, and equal amounts of protein were separated on 4–12% Bis-Tris precast gels (NuPAGE; Life Technologies) and probed with the indicated antibodies. Where indicated, cells were treated with 5 µg/ml DMSO or MG-132. Unsaturated films were scanned at 600 dpi as 16-bit grayscale TIFF-formatted images. The densitometry analysis was performed using ImageJ software (National Institutes of Health). No image adjustments were made before the analysis. Signal intensities were normalized to the loading control from the same gel.

MS

Wip1 was immunoprecipitated from U2OS or HeLa cells using a monoclonal anti-Wip1 antibody (Santa Cruz Biotechnology, Inc.; 2 µg/reaction) immobilized on protein A/G UltraLink resin. Samples were separated by SDS-PAGE and stained by protein stain (GelCode; Thermo Fisher Scientific). Proteins corresponding to both forms of Wip1 were digested in gel by trypsin (Promega) and analyzed by peptide mass fingerprinting (9.4T Apex-Qe; Bruker Daltonics). Mass spectra were analyzed and interpreted using DataAnalysis 4.0 and BioTools 3.2 software (Bruker Daltonics).

Mutational analysis

Genomic DNA was isolated from peripheral blood of high-risk, *BRCA1/2*-negative, familial and/or early onset breast (*n* = 280)/ovarian (*n* = 50) cancer patients, unselected colorectal cancer patients (*n* = 304), and noncancer controls (*n* = 450) as described previously (Pohlreich et al., 2005; Kleibl et al., 2009; Ticha et al., 2010). All patients and controls were Caucasians of the Czech descent that gave written informed consent with the genetic testing approved by local ethics committees. PCR amplicons covering all *PPM1D* exons with flanking intronic sequences were obtained using PCR master mix (High Resolution Melting; Roche) and a real-time PCR system (LightCycler 480; Roche). PCR amplification was performed using the following sets of primers: 5′-GCGAGCGCCTAGTGTGTCTCC-3′ and 5′-GCGCCAAACAAGCCAGGGAAC-3′ (exon 1); 5′-GTTGCCATTTGTATCCTGACAGTG-3′ and 5′-CTTCAGTAAAAGGGACAGTAGTAGGTC-3′ (exon 2); 5′-CAGGAATTTTGGCTTATGCATCTTTG-3′ and 5′-AGTAAGGGTTTAGTTCTGTCTCCTC-3′ (exon 3); 5′-CTGTTGCTGTTGTACTATTAGCTTCC-3′ and 5′-TGCAAAAATCTACCCAAGGTCAATG-3′ (exon 4); 5′-GATACAGATGTAGTGGCAGCTAAATC-3′; and 5′-CGCTAACCAAAGAACTGGTGTC-3′ (exon 5); 5′-TGCCATCCTACTAGCTTCATAAGAAG-3′ and 5′-TTGGTCCATGACAGTGTTTGTTG-3′ (exon 6a); and 5′-TTCCAATTGGCCTTGTGCCTA-3′ and 5′-AAAAAAGTTCAACATCGGCACCA-3′ (exon 6b). Altered DNA sequences were identified by subjecting PCR amplicons corresponding to the exons 2–6 to a high-resolution melting analysis (Roche), and samples with aberrant melting profile were bidirectionally sequenced using a genetic analyzer (ABI 3130; Life Technologies). Direct sequencing analysis was performed for the analysis of exon 1. All identified *PPM1D* alterations were reconfirmed by sequencing

of 53BP1 foci was analyzed as in Fig. 2 B. (C) FLAG–Wip1-FL, -R458X, -L484X, -F534X, or -K535X mutants were immunoprecipitated, and phosphatase activity was determined as in Fig. 2 D. (D) Wip1 expression in leukocytes from a healthy control or the #BRCA1855 patient was analyzed by immunoblotting. The asterisk indicates a cross-reacting band in the blood sample. Note the increased expression level of the truncated Wip1 in leukocytes from cancer patient. (E) Mutation of *PPM1D* was analyzed in microdissected mammary noncancer tissue and in cancer tissue from the #BRCA1855 patient. Error bars indicate standard deviations.

from an independent PCR amplification. The same method was used for the analysis of DNAs isolated from human tumor cell lines. Mutation analysis of amplicon covering exon 6 only was performed in the validation set of another 398 high-risk, *BRCA1/2*-negative breast cancer patients. Mutation analysis in the formalin-fixed, paraffin-embedded breast cancer specimen from a number BRCA1855 patient was performed by sequencing after PCR amplification of exon 6 from DNA isolated from microdissected cancer and noncancer tissue by DNeasy Blood & Tissue kit (QIAGEN).

Online supplemental material

Fig. S1 shows validation of anti-Wip1 antibodies used in this study and data from MS analysis of truncated and FL forms of Wip1 purified from U2OS cells. Fig. S2 demonstrates that the G1 but not G2 checkpoint is affected in cells with truncated Wip1. Table S1 contains data from mutational analysis of the *PPM1D* gene and anamnestic data of *PPM1D* mutation carriers. Online supplemental material is available at http://www.jcb.org/cgi/content/full/jcb.201210031/DC1.

We are thankful to Dr. Staňek for making the Scan^R microscope available, Dr. Novák (Institute of Molecular Genetics, Prague) for MS analysis, and Dr. Zimovjanová and Dr. Novotný (Department of Oncology, General University Hospital in Prague) for help with clinical samples.

This work was supported by the Grant Agency of the Czech Republic (P301/10/1525, P305/12/2485 and 13-18392S), an institutional grant from the Academy of Sciences of the Czech Republic (RVO68378050), the European Commission (Trireme and Biomedreg), Netherlands Genomic Initiative of Nederlandse organisatie voor Wetenschappelijk Onderzoek (Cancer Genomics Center), Dutch Cancer Society (UU2009-4478), Grant Agency of the Ministry of Health of the Czech Republic (NT13343-4), and Charles University in Prague (PRVOUK-P27/LF1/1).

Submitted: 5 October 2012
Accepted: 11 April 2013

References

Agami, R., and R. Bernards. 2000. Distinct initiation and maintenance mechanisms cooperate to induce G1 cell cycle arrest in response to DNA damage. *Cell*. 102:55–66. http://dx.doi.org/10.1016/S0092-8674(00)00010-6

Bartkova, J., Z. Horejsí, K. Koed, A. Krämer, F. Tort, K. Zieger, P. Guldberg, M. Sehested, J.M. Nesland, C. Lukas, et al. 2005. DNA damage response as a candidate anti-cancer barrier in early human tumorigenesis. *Nature*. 434:864–870. http://dx.doi.org/10.1038/nature03482

Bartkova, J., N. Rezaei, M. Liontos, P. Karakaidos, D. Kletsas, N. Issaeva, L.-V.F. Vassiliou, E. Kolettas, K. Niforou, V.C. Zoumpourlis, et al. 2006. Oncogene-induced senescence is part of the tumorigenesis barrier imposed by DNA damage checkpoints. *Nature*. 444:633–637. http://dx.doi.org/10.1038/nature05268

Bulavin, D.V., O.N. Demidov, S.i. Saito, P. Kauraniemi, C. Phillips, S.A. Amundson, C. Ambrosino, G. Sauter, A.R. Nebreda, C.W. Anderson, et al. 2002. Amplification of PPM1D in human tumors abrogates p53 tumor-suppressor activity. *Nat. Genet.* 31:210–215. http://dx.doi.org/10.1038/ng894

Bulavin, D.V., C. Phillips, B. Nannenga, O. Timofeev, L.A. Donehower, C.W. Anderson, E. Appella, and A.J. Fornace Jr. 2004. Inactivation of the Wip1 phosphatase inhibits mammary tumorigenesis through p38 MAPK-mediated activation of the p16(Ink4a)-p19(Arf) pathway. *Nat. Genet.* 36:343–350. http://dx.doi.org/10.1038/ng1317

Castellino, R.C., M. De Bortoli, X. Lu, S.-H. Moon, T.-A. Nguyen, M.A. Shepard, P.H. Rao, L.A. Donehower, and J.Y. Kim. 2008. Medulloblastomas overexpress the p53-inactivating oncogene WIP1/PPM1D. *J. Neurooncol.* 86:245–256. http://dx.doi.org/10.1007/s11060-007-9470-8

Chen, M.-S., J. Hurov, L.S. White, T. Woodford-Thomas, and H. Piwnica-Worms. 2001. Absence of apparent phenotype in mice lacking Cdc25C protein phosphatase. *Mol. Cell. Biol.* 21:3853–3861. http://dx.doi.org/10.1128/MCB.21.12.3853-3861.2001

Di Micco, R., M. Fumagalli, A. Cicalese, S. Piccinin, P. Gasparini, C. Luise, C. Schurra, M. Garre', P.G. Nuciforo, A. Bensimon, et al. 2006. Oncogene-induced senescence is a DNA damage response triggered by DNA hyper-replication. *Nature*. 444:638–642. http://dx.doi.org/10.1038/nature05327

el-Deiry, W.S., T. Tokino, V.E. Velculescu, D.B. Levy, R. Parsons, J.M. Trent, D. Lin, W.E. Mercer, K.W. Kinzler, and B. Vogelstein. 1993. WAF1, a potential mediator of p53 tumor suppression. *Cell*. 75:817–825. http://dx.doi.org/10.1016/0092-8674(93)90500-P

Fiscella, M., H. Zhang, S. Fan, K. Sakaguchi, S. Shen, W.E. Mercer, G.F. Vande Woude, P.M. O'Connor, and E. Appella. 1997. Wip1, a novel human protein phosphatase that is induced in response to ionizing radiation in a p53-dependent manner. *Proc. Natl. Acad. Sci. USA*. 94:6048–6053. http://dx.doi.org/10.1073/pnas.94.12.6048

Gorgoulis, V.G., L.-V.F. Vassiliou, P. Karakaidos, P. Zacharatos, A. Kotsinas, T. Liloglou, M. Venere, R.A. Ditullio Jr., N.G. Kastrinakis, B. Levy, et al. 2005. Activation of the DNA damage checkpoint and genomic instability in human precancerous lesions. *Nature*. 434:907–913. http://dx.doi.org/10.1038/nature03485

Halazonetis, T.D., V.G. Gorgoulis, and J. Bartek. 2008. An oncogene-induced DNA damage model for cancer development. *Science*. 319:1352–1355. http://dx.doi.org/10.1126/science.1140735

Hollstein, M., D. Sidransky, B. Vogelstein, and C.C. Harris. 1991. p53 mutations in human cancers. *Science*. 253:49–53. http://dx.doi.org/10.1126/science.1905840

Jackson, S.P., and J. Bartek. 2009. The DNA-damage response in human biology and disease. *Nature*. 461:1071–1078. http://dx.doi.org/10.1038/nature08467

Kleibl, Z., O. Havranek, I. Hlavata, J. Novotny, J. Sevcik, P. Pohlreich, and P. Soucek. 2009. The CHEK2 gene I157T mutation and other alterations in its proximity increase the risk of sporadic colorectal cancer in the Czech population. *Eur. J. Cancer*. 45:618–624. http://dx.doi.org/10.1016/j.ejca.2008.09.022

Knudson, A.G. 2002. Cancer genetics. *Am. J. Med. Genet.* 111:96–102. http://dx.doi.org/10.1002/ajmg.10320

Le Guezennec, X., and D.V. Bulavin. 2010. WIP1 phosphatase at the crossroads of cancer and aging. *Trends Biochem. Sci.* 35:109–114. http://dx.doi.org/10.1016/j.tibs.2009.09.005

Li, J., Y. Yang, Y. Peng, R.J. Austin, W.G. van Eyndhoven, K.C.Q. Nguyen, T. Gabriele, M.E. McCurrach, J.R. Marks, T. Hoey, et al. 2002. Oncogenic properties of PPM1D located within a breast cancer amplification epicenter at 17q23. *Nat. Genet.* 31:133–134. http://dx.doi.org/10.1038/ng888

Liang, C., E. Guo, S. Lu, S. Wang, C. Kang, L. Chang, L. Liu, G. Zhang, Z. Wu, Z. Zhao, et al. 2012. Over-expression of wild-type p53-induced phosphatase 1 confers poor prognosis of patients with gliomas. *Brain Res.* 1444:65–75. http://dx.doi.org/10.1016/j.brainres.2011.12.052

Lindqvist, A., M. de Bruijn, L. Macurek, A. Brás, A. Mensinga, W. Bruinsma, O. Voets, O. Kranenburg, and R.H. Medema. 2009. Wip1 confers G2 checkpoint recovery competence by counteracting p53-dependent transcriptional repression. *EMBO J.* 28:3196–3206. http://dx.doi.org/10.1038/emboj.2009.246

Lu, X., B. Nannenga, and L.A. Donehower. 2005. PPM1D dephosphorylates Chk1 and p53 and abrogates cell cycle checkpoints. *Genes Dev.* 19:1162–1174. http://dx.doi.org/10.1101/gad.1291305

Macůrek, L., A. Lindqvist, O. Voets, J. Kool, H.R. Vos, and R.H. Medema. 2010. Wip1 phosphatase is associated with chromatin and dephosphorylates gammaH2AX to promote checkpoint inhibition. *Oncogene*. 29:2281–2291. http://dx.doi.org/10.1038/onc.2009.501

Mailand, N., J. Falck, C. Lukas, R.G. Syljuâsen, M. Welcker, J. Bartek, and J. Lukas. 2000. Rapid destruction of human Cdc25A in response to DNA damage. *Science*. 288:1425–1429. http://dx.doi.org/10.1126/science.288.5470.1425

Medema, R.H., and L. Macůrek. 2012. Checkpoint control and cancer. *Oncogene*. 31:2601–2613. http://dx.doi.org/10.1038/onc.2011.451

Mulligan, L.M., J.B.J. Kwok, C.S. Healey, M.J. Elsdon, C. Eng, E. Gardner, D.R. Love, S.E. Mole, J.K. Moore, L. Papi, et al. 1993. Germ-line mutations of the RET proto-oncogene in multiple endocrine neoplasia type 2A. *Nature*. 363:458–460. http://dx.doi.org/10.1038/363458a0

Nannenga, B., X. Lu, M. Dumble, M. Van Maanen, T.-A. Nguyen, R. Sutton, T.R. Kumar, and L.A. Donehower. 2006. Augmented cancer resistance and DNA damage response phenotypes in PPM1D null mice. *Mol. Carcinog.* 45:594–604. http://dx.doi.org/10.1002/mc.20195

Nguyen, T.-A., S.D. Slattery, S.-H. Moon, Y.F. Darlington, X. Lu, and L.A. Donehower. 2010. The oncogenic phosphatase WIP1 negatively regulates nucleotide excision repair. *DNA Repair (Amst.)*. 9:813–823. http://dx.doi.org/10.1016/j.dnarep.2010.04.005

Nishida, T., S. Hirota, M. Taniguchi, K. Hashimoto, K. Isozaki, H. Nakamura, Y. Kanakura, T. Tanaka, A. Takabayashi, H. Matsuda, and Y. Kitamura. 1998. Familial gastrointestinal stromal tumours with germline mutation of the KIT gene. *Nat. Genet.* 19:323–324. http://dx.doi.org/10.1038/1209

Pärssinen, J., E.-L. Alarmo, R. Karhu, and A. Kallioniemi. 2008. PPM1D silencing by RNA interference inhibits proliferation and induces apoptosis in breast cancer cell lines with wild-type p53. *Cancer Genet. Cytogenet.* 182:33–39. http://dx.doi.org/10.1016/j.cancergencyto.2007.12.013

Pohlreich, P., M. Zikan, J. Stribrna, Z. Kleibl, M. Janatova, J. Kotlas, J. Zidovska, J. Novotny, L. Petruzelka, C. Szabo, and B. Matous. 2005. High proportion of recurrent germline mutations in the BRCA1 gene in breast and ovarian cancer patients from the Prague area. *Breast Cancer Res.* 7:R728–R736. http://dx.doi.org/10.1186/bcr1282

Rauta, J., E.-L. Alarmo, P. Kauraniemi, R. Karhu, T. Kuukasjärvi, and A. Kallioniemi. 2006. The serine-threonine protein phosphatase PPM1D is frequently activated through amplification in aggressive primary breast tumours. *Breast Cancer Res. Treat.* 95:257–263. http://dx.doi.org/10.1007/s10549-005-9017-7

Ruark, E., K. Snape, P. Humburg, C. Loveday, I. Bajrami, R. Brough, D.N. Rodrigues, A. Renwick, S. Seal, E. Ramsay, et al; Breast and Ovarian Cancer Susceptibility Collaboration; Wellcome Trust Case Control Consortium. 2013. Mosaic PPM1D mutations are associated with predisposition to breast and ovarian cancer. *Nature*. 493:406–410. http://dx.doi.org/10.1038/nature11725

Saito-Ohara, F., I. Imoto, J. Inoue, H. Hosoi, A. Nakagawara, T. Sugimoto, and J. Inazawa. 2003. PPM1D is a potential target for 17q gain in neuroblastoma. *Cancer Res.* 63:1876–1883.

Sakaue-Sawano, A., H. Kurokawa, T. Morimura, A. Hanyu, H. Hama, H. Osawa, S. Kashiwagi, K. Fukami, T. Miyata, H. Miyoshi, et al. 2008. Visualizing spatiotemporal dynamics of multicellular cell-cycle progression. *Cell*. 132:487–498. http://dx.doi.org/10.1016/j.cell.2007.12.033

Schmidt, L., F.-M. Duh, F. Chen, T. Kishida, G. Glenn, P. Choyke, S.W. Scherer, Z. Zhuang, I. Lubensky, M. Dean, et al. 1997. Germline and somatic mutations in the tyrosine kinase domain of the MET proto-oncogene in papillary renal carcinomas. *Nat. Genet.* 16:68–73. http://dx.doi.org/10.1038/ng0597-68

Ticha, I., Z. Kleibl, J. Stribrna, J. Kotlas, M. Zimovjanova, M. Mateju, M. Zikan, and P. Pohlreich. 2010. Screening for genomic rearrangements in BRCA1 and BRCA2 genes in Czech high-risk breast/ovarian cancer patients: high proportion of population specific alterations in BRCA1 gene. *Breast Cancer Res. Treat.* 124:337–347. http://dx.doi.org/10.1007/s10549-010-0745-y

Vogelstein, B., and K.W. Kinzler. 2004. Cancer genes and the pathways they control. *Nat. Med.* 10:789–799. http://dx.doi.org/10.1038/nm1087

Vogelstein, B., D. Lane, and A.J. Levine. 2000. Surfing the p53 network. *Nature*. 408:307–310. http://dx.doi.org/10.1038/35042675